Liquid Crystals
Publication details, including instructions for authors and subscription information:
http://www.informaworld.com/smpp/title~content=t713926090

Nematic-isotropic interfacial tension anisotropy of a calamitic lyotropic liquid crystal

T. Beica[a]; R. Moldovan Corresponding author[a]; M. Tintaru[a]; M. R. Puica[b]; I. Enache[a]; S. Frunza[a]
[a] National Institute of Materials Physics, R-77125 Bucharest-Magurele, Romania [b] Department of Physics, University Politehnica of Bucharest, R-77206, Romania

Online publication date: 12 May 2010

To cite this Article Beica, T. , Moldovan Corresponding author, R. , Tintaru, M. , Puica, M. R. , Enache, I. and Frunza, S.(2004) 'Nematic-isotropic interfacial tension anisotropy of a calamitic lyotropic liquid crystal', Liquid Crystals, 31: 3, 325 — 332
To link to this Article: DOI: 10.1080/02678290410001648642
URL: http://dx.doi.org/10.1080/02678290410001648642

LIQUID CRYSTALS, VOL. 31, NO. 3, MARCH 2004, 325–332

Nematic–isotropic interfacial tension anisotropy of a calamitic lyotropic liquid crystal

T. BEICA, R. MOLDOVAN*, M. TINTARU, M. R. PUICA†, I. ENACHE and S. FRUNZA

National Institute of Materials Physics, P.O.Box MG-07, R-77125 Bucharest-Magurele, Romania
†Department of Physics, University Politehnica of Bucharest, Spl. Independentei 313, R-77206, Romania

(*Received 25 June 2003; in final form 29 September 2003; accepted 18 October 2003*)

In a planar oriented sample of a calamitic nematic lyotropic system (mixture of sodium lauryl sulphate/water/decanol), isotropic pretransitional domains appear at the nematic to isotropic transition. The domains are oblong in shape with the long axis along the orientational direction. We show experimental evidence that this oblong shape is determined by the nematic–isotropic interfacial tension anisotropy. Two uniparametric models of simple angular dependences for the interfacial tension are tested. Using the differential system obtained from the Young–Laplace condition at the nematic–isotropic interface, the domain shape can be numerically calculated for each value of the interfacial tension anisotropy. By processing the values of the transmitted light through both an isolated isotropic domain and its surrounding nematic zone, we obtain the anisotropy of the interfacial tension as the main fitting parameter. An estimation of the ratio of the extreme values for the interfacial tension is given.

1. Introduction

Amphiphilic molecules, under certain conditions, organize into micellar aggregates that form lyotropic nematic mesophases. These are anisotropic liquids containing micellar aggregates with long range orientational order, but without translational order. The sodium lauryl sulphate (SLS)/water/decanol system, for example, provides lyotropic mixtures that exhibit lyonematic phases and for which all the three possible types of lyonematic phase, calamitic, discotic and biaxial, have been discovered and studied [1–4].

Partial phase diagrams of this lyotropic system for concentrations corresponding to lyonematics, both as a function of concentration for given temperatures and as a function of temperature for given concentrations, have been reported in the literature [4]. On increasing the temperature, the system usually undergoes a variety of phase transitions that includes transformations from one type of lyonematic to an other type or to the isotropic phase. There are indications in the literature [4] that the calamitic (N_C) to isotropic (I) transition usually takes place by passing through a poly-phasic (N_C+I) region, but its temperature range is not well established.

In this paper we report a study of the nematic to isotropic transition of a SLS/water/decanol calamitic system and provide evidence for oblong isotropic domains appearing in oriented samples. Section 2 contains experimental details, including the sample preparation, some experimental observations which allow us to establish the nature of the isotropic domains, and some specific experimental details to ensure that valid results are obtained. In §3 a theory is presented describing the oblong form of the domain based on the anisotropy of the interfacial tension. In §4, two simple phenomenological models for the angular dependence of the interfacial tension are compared for the temperature evolution of a single domain, and for five isolated domains, and the results are discussed.

2. Experimental

2.1. *Sample preparation and experimental set-up*

The lyotropic system studied has the composition by weight %: 25.05 SLS + 70.47 water + 4.48 decanol. It shows a nematic calamitic phase (N_C) in the temperature range 22–29.6°C. The mesophase was prepared using SLS (Merck 99% purity) without additional purification, 1-decanol (Merck, for synthesis) and triply

*Author for correspondence; e-mail: rodi@alpha1.infim.ro

Liquid Crystals ISSN 0267-8292 print/ISSN 1366-5855 online © 2004 Taylor & Francis Ltd
http://www.tandf.co.uk/journals
DOI: 10.1080/02678290410001648642

distilled water. The liquid crystalline mixture was prepared as described elsewhere [5].

The cell used for the measurements consists of two glass plates separated by a frame-shaped glass spacer of 170 μm thickness. The two holes in one of the glass plates used for filling the cell with the lyotropic material were sealed with an indium ball and epoxy resin, preventing any changes in composition of the sample for several weeks. The inner surfaces of the limiting glass plates were previously covered by spin coating with a polystyrene layer from a 1.57 wt% solution in toluene. The polystyrene was dried for 15 min at about 50°C and unidirectionally rubbed. Such a method of obtaining uniform alignment of lyonematics, with the nematic director parallel to the rubbing direction, has been described in the literature [6]. A good uniform planar liquid crystal alignment was obtained by the combined action of the treatment of the glass walls and a magnetic field of 0.5 T applied for 1–2 h, parallel to the rubbing direction.

The liquid crystal cells were placed in a microscope hot stage system (Instec, Inc.), and observed between crossed polarizers set at 45° to the easy direction. The light beam illuminating the sample crosses an interferential filter with $\lambda = 589$ nm. The aspect changes of the sample were observed on heating, using an integrated system with a video camera (Kodak Megaplus, model ES 1.0) connected to a PC. The optic system magnification was calibrated using a stage micrometer. The temperature rate was $0.005°C\,min^{-1}$.

Some microscopic investigations were performed using a home-made temperature controlled micro chamber placed between the poles of an electromagnet.

2.2. *Isotropic domains*

In uniform planar aligned samples, oblong isotropic domains appeared in the nematic matrix at the transition. The isotropic domains were ordered with their major axes approximately parallel to the nematic director. Such oblong isotropic domains were also observed in Vitrocom tubes for which a uniform planar alignment was obtained by capillary flow in the filling process. Covering the glass surfaces with a rubbed polymer ensured a reproducible uniform planar orientation.

The domains grew in number and size with increasing temperature, in the nematic–isotropic coexistence temperature range of 0.1°C before the whole sample became isotropic. This coexistence domain is narrower than the approximately 2°C polyphasic domain at the nematic to isotropic transition, reported by Quist [4].

Figure 1 shows a photo micrograph of an aligned sample at a temperature ≈0.03°C higher than that of the appearance of the first domain. In the figure, the nematic director is horizontal and those of the crossed polarizer axes are set at 45° to the director. One can see that two or more isotropic domains, having different depths of sample thickness, are viewed as overlapping. This suggests that they do not extend over the whole thickness of the sample. One can also observe that many isotropic domains are free and independent entities. Measurements of light transmission on isolated isotropic domains allowed us to observe their evolution, both in time and with temperature.

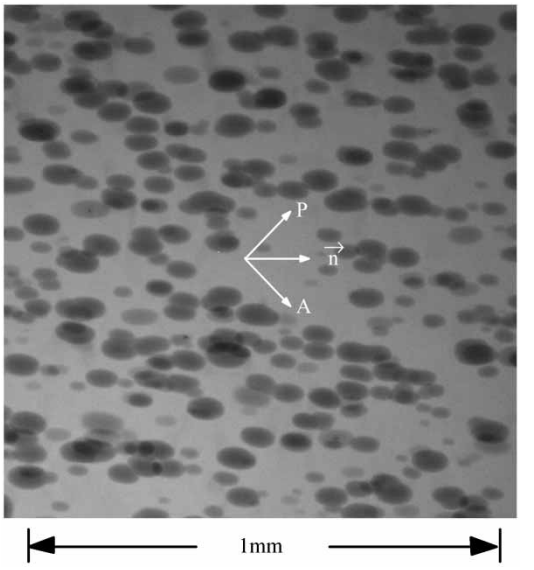

Figure 1. Photomicrograph of isotropic domains in a calamitic nematic matrix for a sample of 170 μm thickness. Temperature is ≈0.03°C higher than for the appearance of the first domain. P, A, $\vec{n}$ are polarizer, analyzer and nematic director, respectively.

2.3. *Possible mechanisms governing the shape of oblong isotropic domains*

The elongated shape of the isotropic domains and their general orientation parallel to the nematic director suggest the involvement of the anisotropic properties of the studied system. The solid–liquid interface anisotropy leads to nematic alignment and there is no direct interaction with the oblong domains as these are significantly thinner than the sample. The oblong domains also appear between untreated surfaces if another alignment mechanism is used.

We will now analyse anisotropic properties that may be involved. The probable factors which could play a key role in determining the shape of the isotropic domains are (i) the interfacial tension anisotropy at the nematic–isotropic interface, and (ii) the local reduction of the transition temperature, as a result of some impurities in the sample. In the latter case, a slow anisotropic diffusion process could explain the oblong

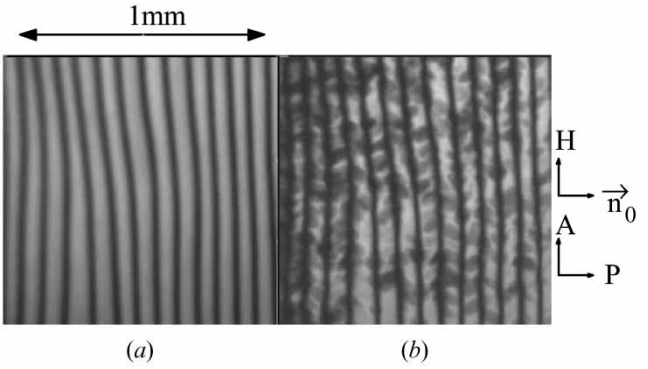

Figure 2. Photomicrographs showing magnetically-induced periodic domains (*a*) without and (*b*) with isotropic domains. P and A are polarizer and analyser, respectively. $\vec{n}_0$ is the nematic director orientation before the application of the magnetic field H.

form, and the isotropic domain shape would represent a map of local transition temperatures. Any relatively fast change of the nematic axis direction would not influence the domain orientation.

To distinguish between the two possible mechanisms, the sample was placed in a magnetic field perpendicular to the nematic orientation. The applied magnetic field induces periodic domains, as reported in the literature [7–9], and the director orientation in this structure is periodically deformed, see figure 2 (*a*). When the isotropic domains appear, their major axes are periodically oriented, in accordance with the nematic director orientation inside the magnetically-induced periodic domains, see figure 2 (*b*).

This experiment shows that the oblong shape of an isotropic domain is the result of the anisotropy of interfacial tension between the nematic–isotropic phases.

2.4. *Experimental requirements*

The system under study consists of an anisotropic matrix and isotropic inclusions separated by an interface. In equilibrium conditions, it is expected that not only is the interface influenced by the orientation of the anisotropic medium, but also that the latter is modified by the interaction with the interface. To obtain reliable data, we have to impose experimental conditions such that the system is in thermal equilibrium (or is close to it). On the other hand a uniform orientation in the nematic volume is desirable. A uniform orientation facilitates both the theoretical treatment of interfacial shape and the calculus of light transmission through sample.

In figure 3, two photomicrographs of domains obtained under different conditions are shown. Figure 3 (*a*) represents an isotropic domain 10 min after its appearance, at a linear heating rate of

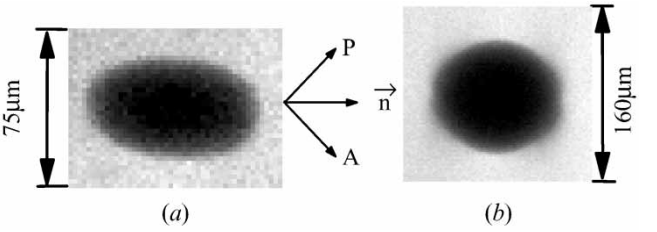

Figure 3. The influence of heating rate on the domain shape. (*a*) Growth at a temperature rate $0.005^{\circ}\mathrm{C\,min^{-1}}$, after $\approx$10 min from its appearance. (*b*) Growth by steps of $0.01^{\circ}\mathrm{C\,h^{-1}}$, after $\approx$5 h from its appearance. Both images have enhanced contrast. P, A, $\vec{n}$ are polarizer, analyser and nematic director, respectively.

$0.005^{\circ}\mathrm{C\,min^{-1}}$; in this time the long axis reached 86 μm. Figure 3 (*b*) shows an isotropic domain obtained under equilibrium conditions, more than 5 h after its appearance, with the temperature in steps of $0.01^{\circ}\mathrm{C\,h^{-1}}$. In the latter case, the domain is 126 μm in length and 112 μm in width/height (i.e. less than the cell thickness of 170 μm).

We observe in figure 3 (*b*) that the form of the domain is less oblong than in the case of figure 3 (*a*). As expected, we also observe a significant perturbation of the nematic orientation in the neighbourhood of the interface.

In figure 3 (*a*), no variation of the nematic orientation in the neighbourhood of the interface is observed. This may be interpreted as follows: since the isotropic domain volume grows with a sufficiently high rate, the region of the nematic volume whose orientation is disturbed by the interface is destroyed. Thus, at the separation surface, the contact between the isotropic medium and the unidirectionally oriented anisotropic medium is permanently ensured.

Thus, the quasi-equilibrium conditions ensured by a relatively slow heating rate ($0.005^{\circ}\mathrm{C\,min^{-1}}$) are more amenable to an easier theoretical description and were chosen for the interfacial tension anisotropy evaluation.

3. Theoretical approach and computational treatment

In our theoretical approach we suppose that the director orientation in the nematic bulk is the same as at the nematic–solid interface (imposed by rubbing). As long as the bulk remains undistorted, the solid–liquid interface gives no contribution to the total free energy.

From the way that the experiment was performed—see §2.4 and figure 3 (*a*)—we also suppose that there is no distortion in the bulk produced by the nematic–isotropic interface. It is possible to fulfil this condition for lyotropic liquid crystals, for which any reorientation process is slow. The bulk, being

undistorted, does not contribute to the free energy of the system.

At the isotropic–nematic interface we assume a weak anchoring coupling. This allows the interface director to have a variable orientation relatively to the interface normal, rather than a fixed direction as in the strong anchoring case. Thus, weak anchoring permits the existence over the whole interface of the same unidirectional orientation as in the bulk if, under the experimental conditions, the bulk orientation is not altered by the interface. For an isotropic–nematic closed interface and weak anchoring, the surface free energy density depends on the angle between the local direction of the interface normal and the direction of the interface director.

In our theoretical treatment we make use of the interfacial tension term instead of the surface free energy density for weak anchoring, because we are dealing with a typical capillarity problem. We will find the relationship between the interfacial tension anisotropy and the domain shape. There are a few references in the literature about interfacial tension measurements at the isotropic–lyotropic interface [10, 11].

The liquid crystal interfacial tension γ depends on the scalar product between the nematic director at the surface $\vec{n}$, and the normal to the interface $\vec{k}$, $\vec{n}\cdot\vec{k}=\cos\phi$. Therefore, γ can be expressed as a power expansion of $\cos\phi$. In the case of nematic liquid crystals that are not polar systems, the odd coefficients in $\cos\phi$ must vanish:

$$\gamma(\phi)=\gamma_0+\gamma_2\cos^2\phi+\gamma_4\cos^4\phi+\ldots+\gamma_{2n}\cos^{2n}\phi. \quad (1)$$

The use of higher terms in the expansion given by equation (1), complicates the simple physical interpretation. In addition a multiparametric model makes any fit too complicated.

To express the angular dependence of interfacial tension, we will try two simple models. In the following theory it will be shown that both become uniparametric models. The models have been chosen to ensure a minimum surface tension (anchoring energy) for normal or tangential anchoring.

Model (a) is similar to the Rapini and Papoular [12] model for anchoring energy, and we call it the RP-model:

$$\gamma(\phi)=\gamma_0+\gamma_2\cos^2\phi=\gamma(0)\cos^2\phi+\gamma(\pi/2)\sin^2\phi \quad (2)$$

where $\gamma(0)$ and $\gamma(\pi/2)$ are the two extreme values of the interfacial tension for the nematic director parallel and perpendicular to the interface normal, respectively. This model is frequently used in weak anchoring studies, for small deviations of the surface orientation from the easy axis.

Model (b) gives an angular dependence similar to that of the extraordinary refractive index in uniaxial crystals. We call it the NE-model:

$$\gamma(\phi)=\frac{\gamma(0)\gamma(\pi/2)}{\left\{[\gamma(0)]^2\sin^2\phi+[\gamma(\pi/2)]^2\cos^2\phi\right\}^{\frac{1}{2}}}. \quad (3)$$

This model is equivalent to the power series from equation (1) where higher terms are implied. It can be used as an approximate phenomenological model, but without a theoretical justification.

We will consider that the form of the isotropic domain surface is obtained by the Young–Laplace condition [13]:

$$\gamma\left(\frac{1}{R_1}+\frac{1}{R_2}\right)=\Delta P \quad (4)$$

where R_1 and R_2 are the two principal curvature radii at each point S of the interface, and ΔP is the corresponding pressure difference. Since in our case the density difference between the two phases is very small [5], we will neglect any hydrostatic contribution to the pressure difference. Under these conditions, the domain shape is axisymmetric, with the symmetry axis parallel to the nematic orientation. The pressure difference is a constant having, at the apex of the oblong domain, the value $\Delta P=2\gamma(0)/R_0$. R_0 is the curvature radius at the apex of the axisymmetric oblong domain, where the two radii of curvature are equal.

Equation (4) can be written in the dimensionless form:

$$\frac{R_0}{R_1}+\frac{R_0}{R_2}=\frac{2\gamma(0)}{\gamma(\phi)}. \quad (5)$$

Because in equation (5) the surface tension contribution is given as a ratio, both simple models, equations (2), (3), can be expressed as a function of a single dimensionless parameter, $\Gamma=\gamma(\pi/2)/\gamma(0)$.

Figure 4 shows the axial section of an isotropic

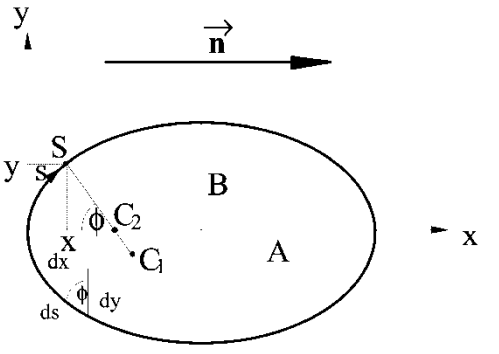

Figure 4. Axial section of an oblong isotropic domain. $\vec{n}$ is the nematic director, ϕ is the angle between the x-axis and the normal to the interface (SC_2C_1); s is the contour length along the profile, A, B are the domain semi axes; $SC_1=R_1$ is the principal curvature radius in the axial section, $SC_2=R_2$ is the principal curvature radius in the normal section.

domain, with the semi-axes A and B, in a coordinate system having the origin in the apex of the domain and the x-axis parallel to its major axis. A parametric form gives a useful representation of the domain axial section $x=x(s)$ and $y=y(s)$, where s is the contour length measured form the apex. Combining equation (5) with the expression for $\gamma(\phi)$ given by (2) or (3), the differential equations obtained are:

$$\frac{d\bar{x}}{d\bar{s}} = \cos\phi \tag{6}$$

$$\frac{d\bar{y}}{d\bar{s}} = \sin\phi \tag{7}$$

$$\frac{d\phi}{d\bar{s}} = \frac{2}{\cos^2\phi + \Gamma\sin^2\phi} - \frac{\sin\phi}{\bar{y}} \tag{8a}$$

$$\frac{d\phi}{d\bar{s}} = 2\left(\sin^2\phi + \Gamma^2\cos^2\phi\right)^{\frac{1}{2}} - \frac{\sin\phi}{\bar{y}} \tag{8b}$$

where $\bar{x}=x/R_0$, $\bar{y}=y/R_0$ and $\bar{s}=s/R_0$ are dimensionless coordinates.

To determine the interface shape for a settled value of Γ, the differential system given by equations (6)–(8) has to be solved with the initial condition

$$\bar{x}(0)=\bar{y}(0)=\phi(0)=0.$$

We used a Runge–Kutta algorithm for numerical integration, with 50 equal intervals, $d\bar{s}$, adjusting the value of $d\bar{s}$ so that $\phi_{50}=\pi/2$. Thus a set of reduced coordinates $\bar{x}_i$, $\bar{y}_i$ with $i=0, \ldots, 50$, is determined. The values of $\bar{x}_{50}$ and $\bar{y}_{50}$ represent exactly the semi-axes values (A, B) of the domain, in R_0 units.

Making $\bar{X}_i=1-\bar{x}_i/\bar{x}_{50}$ and $\bar{Y}_i=\bar{y}_i/\bar{x}_{50}$, the profile description is obtained in new reduced coordinates in the units of the major semi-axis A. The semi-axis A can be more easily evaluated than the curvature radius R_0. In addition, the new set of values is related to a coordinate system having the origin in the domain centre and with the X-axis parallel to the major semi-axis.

We will now describe the algorithm that gives by interpolation any reduced value $\bar{Y}(\bar{X}, \Gamma)$. To obtain intermediate points of the profile, we used a circle arcs interpolation method. For a $\bar{X}$ coordinate we search for the nearest neighbour $\bar{X}_j$ from the series $\bar{X}_1, \ldots, \bar{X}_{49}$, and then a circle is drawn through the three points $(\bar{X}_{j-1}, \bar{Y}_{j-1})$, $(\bar{X}_j, \bar{Y}_j)$, $(\bar{X}_{j+1}, \bar{Y}_{j+1})$. From the corresponding equation of the circle, $\bar{Y}(\bar{X}, \Gamma)$ value is calculated. For $\bar{X}\in[\bar{X}_0, \bar{X}_1]$ the third point is $(\bar{X}_1, -\bar{Y}_1)$, and for $\bar{X}\in[\bar{X}_{49}, \bar{X}_{50}]$ the third point is $(-\bar{X}_{49}, \bar{Y}_{49})$.

Let (X, Y) be the coordinate at a pixel on the image capture device (CCD). For the image of an isotropic domain with its centre at the point ($X0$, $Y0$), and the azimuth angle α between the A semi-axis and X-axis, the reduced coordinates of an (X, Y) image point are:

$$X_{red} = \frac{|(X-X0)\cos\alpha + (Y-Y0)\sin\alpha|}{A}, \tag{9a}$$

$$Y_{red} = \frac{|-(X-X0)\sin\alpha + (Y-Y0)\cos\alpha|}{A}. \tag{9b}$$

Taking into account the revolution symmetry of the domain around the X-axis, the thickness Z corresponding to a point (X, Y), inside the domain, is:

$$Z(X, Y) = 2A\left\{[\bar{Y}(X_{red}, \Gamma)]^2 - Y_{red}^2\right\}^{\frac{1}{2}} \tag{10}$$

where X_{red} and Y_{red} are defined by equations (9). The $\bar{Y}(X_{red}, \Gamma)$ value is obtained using the algorithm described and represents the revolution radius at X_{red} 'latitude'.

Experimentally, we studied the optical transmission of a region containing an isotropic domain. For a uniaxial liquid crystal in a uniform planar aligned sample, placed between crossed polarizers at 45° from the optical axis, the light transmission is given by $T=I\sin^2(\pi\Delta n\cdot W/\lambda)$, where W is the thickness of the sample, Δn is the optical anisotropy, and I is proportional to the incident light intensity. The oblong isotropic domains, of variable thickness $Z(X, Y)$, must be extracted from the nematic matrix thickness. The non-uniformity of image illumination must also, be taken into account. For a small region centred on the point ($X0$, $Y0$), the illumination can be considered as:

$$I(X, Y) = I_0[1 + p_{X0}(X-X0) + p_{Y0}(Y-Y0)] \tag{11}$$

where $I_0=I_0(X0, Y0)$, and p_{X0}, p_{Y0} are the fitting parameters.

The fitting function of light transmission T in an (X, Y) image point, representing an isotropic domain and its surrounding, becomes:

$$T(X, Y) = I(X, Y)\sin^2\left[\frac{\pi\Delta n}{\lambda}(W-Z)\right] \tag{12}$$

where

$$Z = Z(X, Y, X0, Y0, \alpha, A, \Gamma)$$

is the isotropic domain thickness that is given by equation (10) inside the domain and is zero outside of it. As it can easily be seen, the theoretical function $T(X, Y)$ depends on 10 parameters. Among them, only p_{X0}, p_{Y0}, α, $X0$, $Y0$, Δn, A and Γ are variables, while Δn, A and Γ are of interest in our study. In order to obtain these parameters, the function

$$\chi^2 = \sum[T(X, Y) - E(X, Y)]^2$$

must be minimised. $E(X, Y)$ represents the experimental value of transmission corresponding to a pixel and the

summation is over a rectangle of $N \approx 10^3$ pixels, centred approximately on the isotropic domain.

On the basis of the theory described, a computer program was used to analyse the evolution of the isotropic domains on images taken at different temperatures. In addition to the fitting parameters, the program gives two other pieces of useful information for comparing the models:

(1) Standard deviation $\sigma \approx (\chi^2)^{1/2}/N$, corresponding to a domain image fit. This value is useful for directly comparing the different models.
(2) An error distribution map, corresponding to an image, organized as a normalized bitmap with 256 grey levels. A pixel in this bitmap represents the error associated with the corresponding original pixel. Its value reaches 255 (white) if this error has the maximum positive error value and becomes zero (black) for the minimum negative error value. This error map provides a way to evaluate the spatial distribution of errors.

4. Results and discussion

In the preceding section we proposed two simple types of dependence for the interfacial tension, γ as a function of the angle ϕ between the director and the normal to the interface. Both approximations depend on a single dimensionless parameter having a direct physical significance, Γ (the ratio of two extreme interfacial tensions). If this parameter is a material constant (independent of other variables, such as temperature) its value has to be independent of: (a) the moment in time of its determination in the evolution of a domain with temperature; (b) the position of the investigated domain; measurements of different domains should produce close values.

We analysed the temperature evolution of a large number of domains, identified by the position of their centre ($X0$, $Y0$) on the registered images. Not all were taken into consideration, for two reasons. Firstly, during its evolution, the domain must have no other domain in its vicinity. Secondly the first condition has to be fulfilled for a sufficient number of successive images (minimum 10) of the respective domain in its temperature evolution. Images of too small domains ($\leqslant 10$ pixels or $\leqslant 10\,\mu$m, major semi-axis) were discarded for the reason that they contain an insufficient number of pixels for reliable fit. Only five isolated domains were analysed in their evolution with temperature at an interval of minimum 0.06°C.

In this section, we will compare the two models. This will be performed on three levels: (a) the level of the image for one domain at a given temperature; (b) the level of evolution of a domain with the temperature as long as it fulfils the conditions described; (c) the level of all the domains analysed, in accordance with described criteria.

The evolution of the isotropic domain's dimensions and the variation with temperature of the optical anisotropy of the lyonematic in the nematic–isotropic coexistence range, are shown at the end of the section. First we will examine the results of fitting with the RP and NE models for the image of a domain from the five analysed, in accordance with criteria-described. We chose an image in the middle of the domain evolution. These results are shown in figure 5 as error maps and as theoretical profiles corresponding to the fit with the two models. We note that the NE model, figure 5 (*b*), produces more rounded profiles in the apex region than the RP model, figure 5 (*a*). The profiles produced by the NE model are closer to the domain form, shown in figure 5 (*c*) by enhanced contrast image. Standard deviations produced by the fit with the two models for the same image, $\sigma_{RP} = 2.93$ and $\sigma_{NE} = 2.59$; as well as the spatial distribution of errors suggests that the NE model is a better representation.

We will consider now the evolution with temperature/time of the domain shown in figure 5 (*c*). The fit with the two models again favours the NE model, this producing standard deviations for the image σ smaller than the RP model, in the whole domain of evolution, see figure 6 (*c*). The mean values of the interfacial tension ratio given by the fit with the two models are $\Gamma_{RP} = 6.245 \pm 0.413$ and $\Gamma_{NE} = 2.337 \pm 0.029$. By its relative deviation of only 1.2%, the NE model is again favoured in comparison with the RP model, which has a value of 6.6%.

In figure 7 we show the temperature dependence of the interfacial tension ratio Γ for all five isotropic

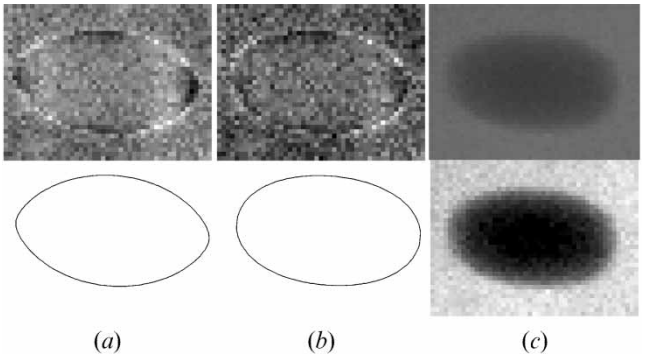

Figure 5. Comparative fits for both models applied on the same domain. (*a*) Error distribution map (upper) and theoretical profile (lower) produced by fit with RP model. (*b*) Error distribution map (upper) and theoretical profile (lower) produced by fit with NE model. (*c*) Original bitmap (upper) of the domain and its enhanced contrast (lower).

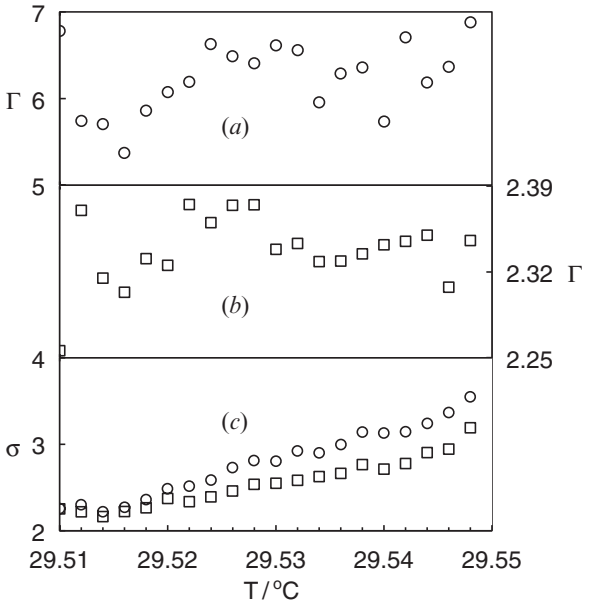

Figure 6. Comparative results obtained from fits using the RP (circles) and NE models (squares). (*a*), (*b*) The interfacial tension ratio Γ vs. temperature. (*c*) Standard deviations σ for the images.

domains investigated. The mean values of interface tension ratios given by the fits with the two models are $\Gamma_{RP}=4.73\pm1.04$ and $\Gamma_{NE}=2.267\pm0.086$. The relative deviation for the mean value produced by the RP model is 22%. This mainly arises from the scattering of values from domain to domain. In figure 7 (*a*) the existence of a Γ dependence on temperature is also suggested. This contributes to the increase in the relative deviation produced by the RP model. The NE model has a mean value with a relative deviation of only 3.8% and thus remains the preferred model. Figure 7 (*b*) does not suggest the existence of a temperature dependence for the ratio Γ in the case of the NE model.

That the RP model produces poorer results than the NE model is understandable, taking into account that it represents only the first two terms in the power expansion from equation (1). Models of the Rapini–Papoular type are adequate for small deviations of the director orientation at the surface from the easy direction (which can be normal or tangential at the surface). In our case $\phi\in[0,\pi/2]$, and hence the RP model is an inadequate approximation. It would be necessary to use higher terms in the expansion given by equation (1), but this, on the one hand makes the fit too complicated, while on the other complicates the simple physical interpretation. Although it is characterized by just a single constant (the ratio Γ), the NE model is equivalent to a power series with higher terms.

Examining the results described, we can estimate that the value

$$\Gamma=\gamma(\pi/2)/\gamma(0)=2.27\pm0.09$$

describes the anisotropy of the interfacial tension at the nematic to isotropic interface for the SLS/water/decanol lyotropic system. A value for the ratio of the extreme interfacial tensions of 1.5 was obtained by Sallen *et al.* [10] for the hexagonal–isotropic interface of the lyotropic $C_{12}EO_2$/water mixture. We note that the value of Γ greater than one shows that the smallest anchoring energy at the nematic–isotropic interface is reached for $\phi=0$. Thus the normal direction represents the easy axis at the nematic–isotropic interface.

Our computer program allows for the dimensional determination of the domains. As can be seen from figure 8, in all cases the major semi-axis grows linearly with temperature, having approximately the same growth rate. We note that in the nematic–isotropic coexistence temperature range, the domain major semi-axis A grows significantly while Γ remains essentially constant, see figure 7 (*b*).

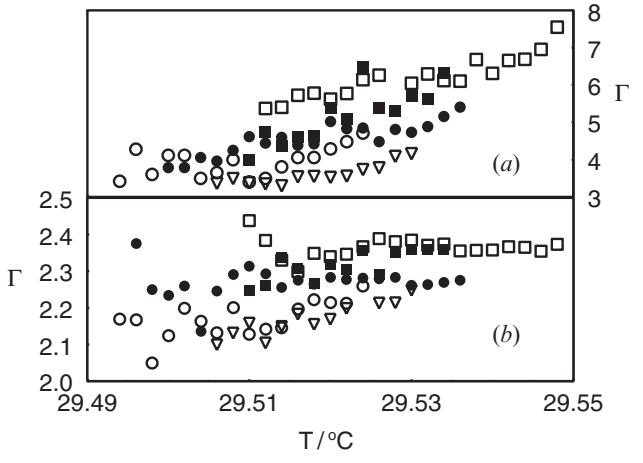

Figure 7. The interfacial tension ratio Γ vs. temperature for five isolated isotropic domains. (*a*) RP model, (*b*) NE model.

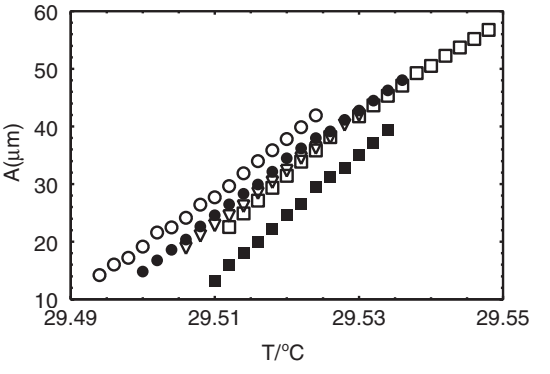

Figure 8. The major semi-axis A vs. temperature for five isolated isotropic domains.

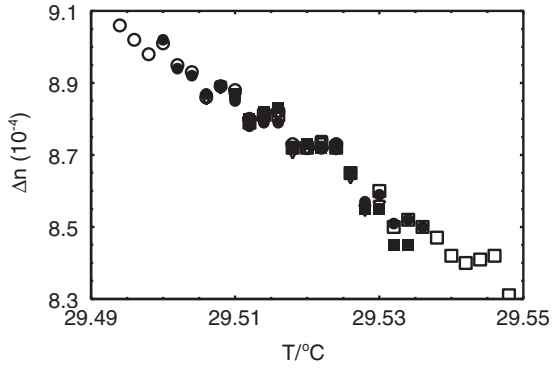

Figure 9. Optical anisotropy Δn vs. temperature for five isolated domains.

We also determined the temperature dependence of the optical anisotropy near the nematic to isotropic transition. It was found, as expected, that the optical anisotropy decreases as temperature increases, see figure 9. The order of magnitude for Δn values is in accord with those reported in the literature for other lyotropic systems [14–17]. The values smaller than 10^{-3} obtained in this experiment at the nematic to isotropic transition, are in good agreement with those obtained by us for the same system in the nematic range using an interferometric method [18].

The authors thank the Romanian Ministry of Education and Research for financial support under the CERES Project No.32/2001.

References

[1] Amaral, L. Q., and Helene, M. E. M., 1988, *J. phys. Chem.*, **92,** 6094.
[2] Quist, P.-O., and Halle, B., 1993, *Phys. Rev. E*, **47,** 3374.
[3] Quist, P.-O., Fontell, K., and Halle, B., 1994, *Liq. Cryst.*, **16,** 2335.
[4] Quist, P.-O., 1995, *Liq. Cryst.*, **18,** 623.
[5] Beica, T., Moldovan, R., Puica, M. R., and Frunza, S., 2002, *Liq. Cryst.*, **29,** 1275.
[6] Bonvent, J. J., Bechtold, I. H., Vega, M. L., and Oliveira, E. A., 2000, *Phys. Rev. E*, **62,** 3775.
[7] Chavrolin, J., and Hendrikx, Y., 1980, *J. Physique Lett.*, **41,** L-597.
[8] Kroin, T., and Figueiredo Neto, A. M., 1987, *Phys. Rev. A*, **36,** 2987.
[9] Simões, M., Palangana, A. J., and Evangelista, L. R., 1996, *Phys. Rev. E*, **54,** 3765.
[10] Sallen, L., Oswald, P., Géminard, J. C., and Malthête, J., 1995, *J. Phys. II (F.)*, **5,** 937.
[11] Sallen, L., 1996, PhD. thesis, L'Ecole Normale Supérieure de Lyon, France.
[12] Rapini, A., and Papoular, M., 1969, *J. Phys. (Paris) Colloq.*, **30,** C4–54.
[13] Adamson, A. W., 1990, *Physical Chemistry of Surfaces* (New York: Wiley-Interscience), pp. 4–52.
[14] Galerne, Y., and Marcerou, J. P., 1983, *Phys. Rev. Lett.*, **51,** 2109.
[15] Larson, B. D., and Litstern, J. D., 1984, *Mol. Cryst. liq. Cryst.*, **113,** 13.
[16] Oliveira, E. A., and Figueiredo Neto, A. M., 1994, *Phys. Rev. E*, **49,** 629.
[17] Pinto, A. V. A., and Barbosa, A. A., 1998, *Mol. Cryst. liq. Cryst. Sci. Technol., Sect. A*, **309,** 45.
[18] Beica, T., Moldovan, R., Tintaru, M., Enache, I., and Frunza, S., 2004, *Cryst. Res. Technol*, **39,** 149.